CHANSON, H., and TAN, K.K. (2010). "Turbulent Mixing of Particles under Tidal Bores: an Experimental Analysis." *Journal of Hydraulic Research*, IAHR, Vol. 48, No. 5, pp. 641-649 (DOI: 10.1080/00221686.2010.512779 (ISSN 0022-1686).

# Turbulent mixing of particles under tidal bores: an experimental analysis

Hubert Chanson
The University of Queensland, School of Civil Engineering, Brisbane QLD 4072, Australia
Email: h.chanson@uq.edu.au (Author for corresponence)
and Kok-Keng Tan
The University of Queensland, School of Civil Engineering, Brisbane QLD 4072, Australia

## Abstract

A tidal bore develops in an estuary when the tidal range exceeds 4.5 to 6 m and the estuarine bathymetry amplifies the tidal wave. The bore is an abrupt rise in water depth associated with a discontinuity in velocity and pressure fields at the front. Herein the free-surface properties and the turbulent mixing of light-weight particles were investigated during the passage of tidal bores. The free-surface properties were recorded using a non-intrusive technique, while some particle tracking was performed under undular and breaking bores. A basic result was the identification of a broad spectrum of particle trajectories, linked with the existence of large-scale vortical structures. These turbulent structures were responsible for the vertical mixing of the water column when a tidal bore propagates upstream in an estuary. The large-scale eddies were also responsible to the rapid longitudinal dispersion of particulates, such as fish eggs, with some form of preferential motion depending upon the particle's vertical elevation.

Keywords: Particle dispersion, Physical modelling, Tidal bores, Turbulent mixing, Unsteady flow measurements.

## 1. Introduction

A bore is an unsteady flow motion generated by the rapid water level rise at the river mouth during the early flood tide. With time, the leading edge of the tidal wave becomes steeper and steeper until it forms a wall of water: i.e., the tidal bore. After the formation of the bore, there is an abrupt rise in water depth at the bore front that is discontinuity in water depth and velocity field. Figure 1 shows the tidal bore of the Garonne River in south-western France. Once formed, the flow properties immediately before and after the tidal bore must satisfy the continuity and momentum principles (Rayleigh 1908, Henderson 1966, Liggett 1994). The integral form of the equations of conservation of mass and momentum gives a series of relationships between the flow properties in front of and behind the bore front. For a rectangular horizontal channel and neglecting bed friction, it yields:

$$\frac{d_{conj}}{d_o} = \frac{1}{2}\left(\sqrt{1+8\,\mathsf{F}^2}-1\right) \quad (1)$$

where $d_o$ is the initial water depth, $d_{conj}$ is the conjugate flow depth immediately after the bore passage, $\mathsf{F}$ is the tidal bore Froude number defined as:

$$\mathsf{F} = \frac{V_o + U}{\sqrt{g\,d_o}} \quad (2)$$

with $V_o$ the initial river flow velocity positive downstream and $U$ is the tidal bore celerity for an observer standing on the bank positive upstream (Fig. 2A). The Froude number of the tidal bore is always greater than unity. For $\mathsf{F} < 1$, the tidal wave cannot become a tidal bore. For Froude numbers slightly greater than unity, an undular bore is observed: the bore leading edge is followed by a train of secondary waves (Fig. 1). For larger Froude numbers, a marked turbulent roller is seen: i.e., a breaking tidal bore.

Historically, some major contributions on tidal bores included the works of Bazin (1865), Barré de Saint Venant (1871), Boussinesq (1877), Benjamin and Lighthill (1954) and Peregrine (1966). More recently, some unsteady turbulence measurements were conducted using PIV and ADV techniques (Hornung et al. 1995, Koch and Chanson 2009, Chanson 2010). The results showed some intense turbulent mixing during the tidal bore front passage.

In this study, the free-surface properties and the turbulent mixing of light particles were investigated during the passage of tidal bores. The tracking of particles was conducted with both undular and breaking bores to provide some new Lagrangian description of the particle mixing processes. The results complement earlier Eulerian velocity measurements performed in the same facility (Koch and Chanson 2009, Chanson 2010), and give a new understanding of the turbulent mixing of particulates such as light-weight sediment materials and fish eggs.

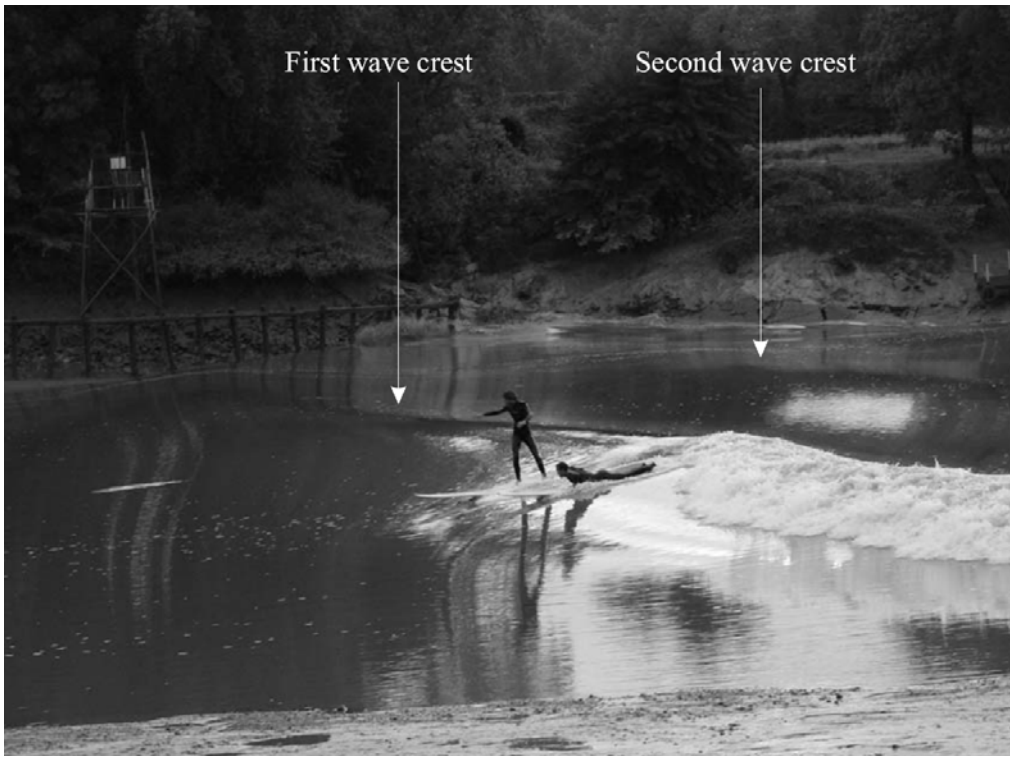


Fig. 1 - Photograph of the undular tidal bore of the Garonne River on 1 October 2008 at Béguey (France) - The surfers are riding ahead of the first wave crest with the bore propagating from right to left - Note some wave breaking in the right foreground corresponding to some shallow waters and the first two wave crests in the middle and right background of the photograph

## 2. Experimental facilities

The experiments were performed in a 12 m long 0.5 m wide rectangular open channel test section at the University of Queensland (Fig. 2). The flume was horizontal and made of smooth PVC bed and glass walls. The water was supplied by a constant head tank feeding a large intake basin (2.1 m long, 1.1 m wide, 1.1 m deep) leading to the test section through a bed and sidewall convergent. A radial gate was installed at the channel downstream end ($x$ = 11.9 m where $x$ is the longitudinal distance from the channel test section upstream end), and the gate was used to control the initial water depth $d_o$. A fast-closing tainter gate was located at $x$ = 11.15 m and the gate was closed rapidly to generate the tidal bore propagating upstream in the channel (Fig. 2A).

The initially steady discharge was measured with two orifice meters that were designed based upon the British Standards (1943). In steady flows, the water depths were measured using rail mounted pointer gauges. The bore propagation was studied with a series of acoustic displacement meters Microsonic™ Mic+25/IU/TC located along the channel between $x$ = 10.8 and 4 m and placed above the free-surface (Fig. 2B). Further observations were recorded between $x$ = 5.65 and 4.85 m using a digital video camera Panasonic NV-GS300 (30 fps) and several digital still cameras.

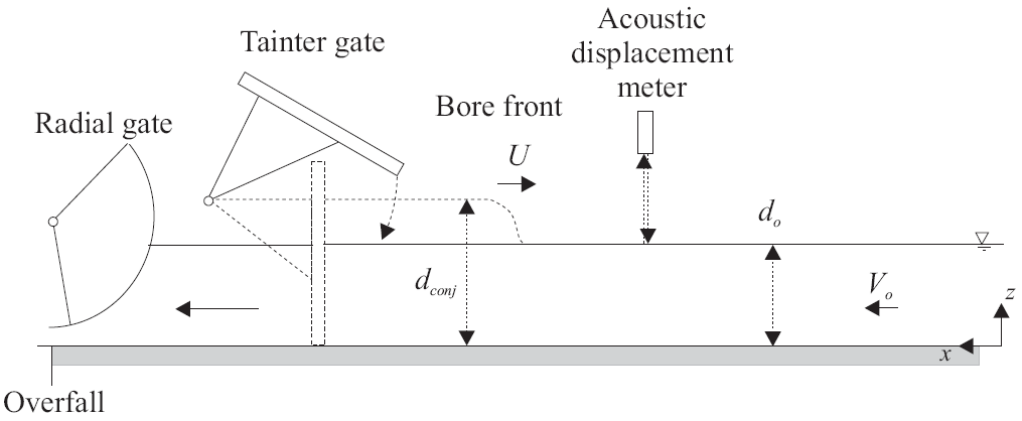


(A) Definition sketch

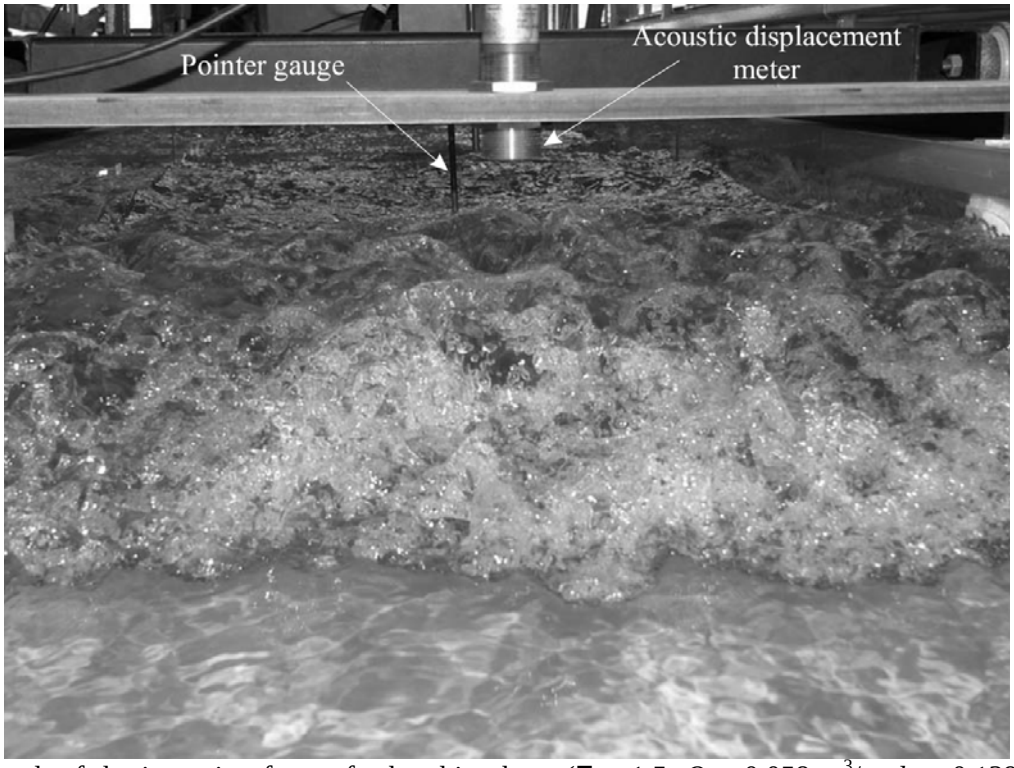


(B) Photograph of the incoming front of a breaking bore (F = 1.5, $Q$ = 0.058 m$^3$/s, $d_o$ = 0.139 m, shutter speed: 1/80 s) - Note the displacement meter sensor above the bore front and a pointer gauge in background

Fig. 2 - Experimental channel

2.1 Particles and particle tracking experiments

For one initial discharge, the turbulent mixing of particles was systematically investigated with both undular and breaking bores (Table 1). The particles were some spherical-shaped beads with an average diameter of 3.72 mm ±0.2 mm. Their relative density was deduced from some particle fall velocity experiments conducted in a 2.0 m high, 0.10 m ∅ water column filled with tap water. The experimental observations yielded a particle fall velocity $w_s$ = 0.047 ±0.012 m/s corresponding to a relative particle density $s$ = 1.037 ±0.012.

The present particle shape, size and density were close to those of striped bass (*Morone saxatilis*) fish eggs. In the Bay of Fundy, the study of Rulifson and Tull (1999) reported some fish egg diameters of about 4 mm with a specific density s between 1.0016 and 1.0066 depending upon their stages of development. Field observations indicated that the lightest eggs were unfertilised water hardened eggs; fertilised eggs less than 10 hours old had a relative density of 1.0029 and the heaviest eggs were in the final stages of development (Rulifson and Tull 1999).

CHANSON, H., and TAN, K.K. (2010). "Turbulent Mixing of Particles under Tidal Bores: an Experimental Analysis." *Journal of Hydraulic Research*, IAHR, Vol. 48, No. 5, pp. 641-649 (DOI: 10.1080/00221686.2010.512779 (ISSN 0022-1686).

Herein the particles were injected on the channel centreline and advected downstream by the initially steady flow. Their turbulent mixing in the bore front was recorded through the glass sidewall between $x$ = 5.65 and 4.85 m using the video camera.

2.2 Generation of the tidal bores

A range of experimental flow conditions were generated by changing independently three parameters: the initially steady discharge $Q$, the initial flow depth $d_o$ and the tainter gate opening after closure (Table 1). The initially steady discharges ranged between 0.013 and 0.058 $m^3/s$. For each test, the opening of the downstream radial gate controlled the initial steady flow depth $d_o$. The radial gate position did not change during an experiment.

The tidal bore was generated by the rapid closure of the downstream tainter gate. The gate was similar to that used by Koch and Chanson (2009) and Chanson (2010). Its closure time was recorded between 0.1 and 0.15 s, and always less than 0.2 s. After the rapid gate closure, the bore propagated upstream (Fig. 2) and each experiment was stopped when the tidal bore front reached the upstream intake structure ($x$ < 0) to avoid any wave reflection in the test section.

Table 1 - Physical modelling and turbulence measurements in tidal bores

| Reference | $Q$ ($m^3/s$) | $d_o$ (m) | $U$ (m/s) | F | Bed roughness | Remarks |
|---|---|---|---|---|---|---|
| (1) | (2) | (3) | (4) | (5) | (6) | (7) |
| Hornung et al. (1995) | 0 | -- | -- | 1.5 to 6 | Smooth | Rectangular channel. |
| Koch & Chanson (2009) | 0.040 | 0.079 | 0.14 to 0.68 | 1.3 to 2.0 | Smooth PVC | $B$ = 0.5 m. |
| Chanson (2010) | 0.058 | 0.137 | 0.56 to 0.9 | 1.17 to 1.5 | Smooth PVC | $B$ = 0.5 m. |
| | | 0.142 | 0.50 to 0.9 | 1.1 to 1.5 | Rough plastic screens | |
| Present study | | | | | Smooth PVC | $B$ = 0.5 m. |
| | 0.013 | 0.0775 | 0.67 | 1.15 | | Particle tracking experiments. |
| | | 0.0505 | 0.55 | 1.51 | | |
| | 0.025 | 0.074 | 0.41-0.68 | 1.29-1.64 | | Free-surface measurements. |
| | | 0.080 | 0.38-0.75 | 1.18-1.51 | | |
| | | 0.107 | 0.42-0.90 | 1.02-1.39 | | |
| | | 0.108 | 0.60-0.71 | 1.10-1.34 | | |
| | | 0.151 | 0.93-1.19 | 1.08-1.2 | | |
| | 0.040 | 0.099 | 0.33-0.71 | 1.20-1.68 | | |
| | | 0.122 | 0.51-0.96 | 1.08-1.47 | | |
| | | 0.140 | 0.66-1.05 | 1.08-1.39 | | |
| | | 0.167 | 0.80-1.05 | 1.06-1.38 | | |
| | | 0.1835 | 0.90-1.18 | 1.01-1.23 | | |
| | 0.058 | 0.1315 | 0.46-0.90 | 1.28-1.70 | | |
| | | 0.155 | 0.54-0.94 | 1.10-1.36 | | |
| | | 0.168 | 0.58-0.92 | 1.04-1.27 | | |
| | | 0.176 | 0.71-1.11 | 1.12-1.37 | | |
| | | 0.195 | 0.82-0.92 | 1.09-1.18 | | |

Notes: $B$: channel width; $d_o$: initial water depth; F: tidal bore Froude number; $Q$: initially steady flow rate; $U$: tidal bore celerity; (--) : data not available. All experiments were conducted with tap water.

## 3. Basic flow patterns and free-surface characteristics

Some visual observations and free-surface measurements were conducted for a range of flow conditions with initially steady subcritical open channel flow (Table 1). Figure 3 presents some typical free-surface records for two Froude numbers (F = 1.2 & 1.56). Several flow patterns were observed depending upon the tidal bore Froude number. For a tidal bore Froude number between unity and 1.5 to 1.6, the tidal bore was

undular. The wave front was followed by a train of quasi-periodic waves called undulations (Fig. 1 & 3A). For larger Froude numbers, a breaking bore was observed (Fig. 2B & 3B). The present observations were consistent with the earlier findings of Favre (1935), Benet and Cunge (1971), Treske (1994) and Hornung et al. (1995).

The undular tidal bore had a smooth, quasi-two-dimensional free-surface profile for $F < 1.2$ to 1.25. For 1.2 to 1.25 < $F$, some slight cross-waves (shock waves) were observed, starting next to the sidewalls upstream of the first wave crest and intersecting next to the first crest on the channel centreline. For 1.35 < $F$ < 1.5 to 1.6, some slight wave breaking was observed at the first wave crest, and the secondary waves were flatter. The findings were comparable to those of earlier studies (Koch and Chanson 2009, Chanson 2010).

At the largest bore Froude numbers (i.e. $F > 1.5$ to 1.6), the bore had a marked roller, and appeared to be quasi-two-dimensional. Behind the roller, the free-surface was about horizontal although large free-surface fluctuations were observed (Fig. 3B). Some air entrainment and intense turbulent mixing was observed in the bore roller.

Note that the flow patterns were basically independent of the initially steady flow rate $Q$ and initial water depth $d_o$, while an earlier study showed that these were also independent of the bed roughness (Chanson 2010).

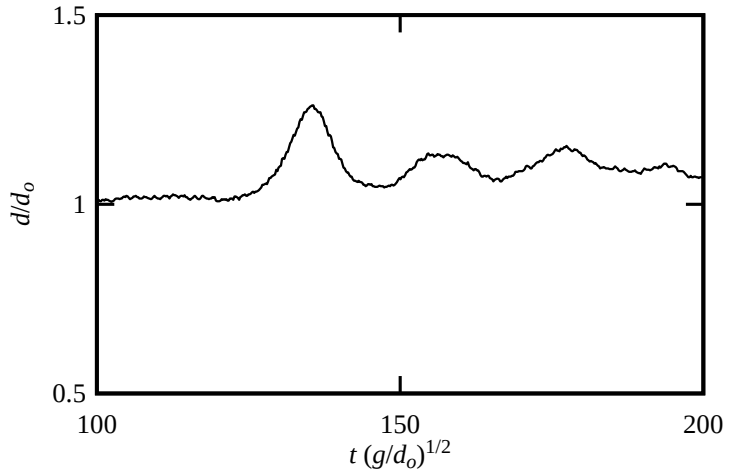


(A) Undular tidal bore - $F = 1.20$, $Q = 0.025$ m$^3$/s, $d_o = 0.107$ m, $U = 0.73$ m/s

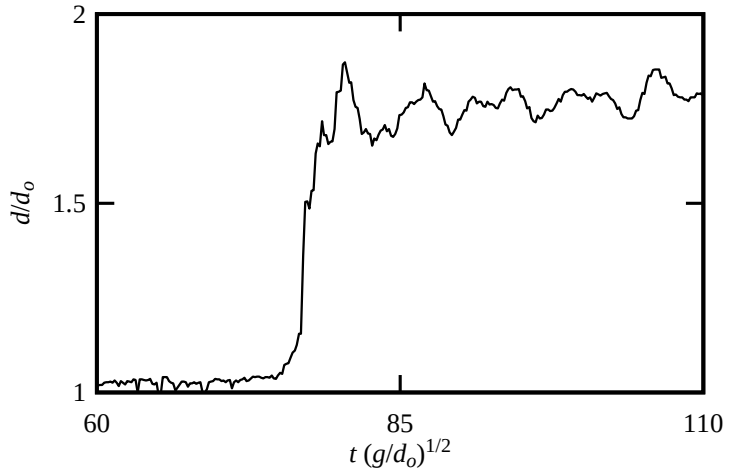


(B) Breaking tidal bore - $F = 1.56$, $Q = 0.058$ m$^3$/s, $d_o = 0.1315$ m, $U = 0.99$ m/s

Fig. 3 - Dimensionless free-surface profiles of tidal bores (measurements at $x = 5$ m)

3.1 Free-surface properties

In a tidal bore, the ratio of water depths $d_{conj}/d_o$ had to satisfy the momentum principle (Eq. (1)). The experimental data are regrouped in Figure 4, where the ratio of the conjugate depths is plotted as a function

of the tidal bore Froude number F. The present data were compared with earlier studies including a field experiment. The data trend was close to that predicted by the momentum principle, although Equation (1) was developed assuming a hydrostatic pressure distribution. Such an approximation is inaccurate in an undular bore since the pressure distributions deviate from hydrostatic because of the streamlines curvatures (Rouse 1946, Montes and Chanson 1998, Cunge 2003).

A key feature of undular tidal bores was the quasi-periodic appearance of the secondary waves (Fig. 1 & 3A). Herein the characteristics of the undulations were systematically recorded for three discharges ($Q$ = 0.025, 0040 & 0.058 $m^3/s$) and for a range of initial flow depths (Table 1). Some typical results are shown in Figures 5 and 6 in terms of the dimensionless wave length $L_w/d_o$ and steepness $a_w/L_w$, where $a_w$ and $L_w$ are respectively the wave amplitude and length. The legend is the same for Figures 4, 5 and 6. The present experimental data are compared with the linear wave theory and Boussinesq equation solutions (Lemoine 1948, Andersen 1978) in Figures 5 and 6. There was a reasonable agreement between the data and theoretical developments, although the wave steepness data were closer to the linear wave theory. While the wave length decayed exponentially with increasing Froude number, the wave steepness data exhibited a local maximum about F = 1.3 to 1.4. It is believed that the apparition of some slight breaking at the first wave crest for F > 1.35 was responsible for the lesser energy dissipated in the secondary wave motion at larger Froude numbers and hence the smaller wave steepness for F > 1.3 to 1.4.

An important finding of the experiments was the independence of the results from the initially steady flow Froude number (Fig. 4 to 6). The free-surface properties were basically independent of the initial water depth and velocity within the range of the experiments (Table 1).

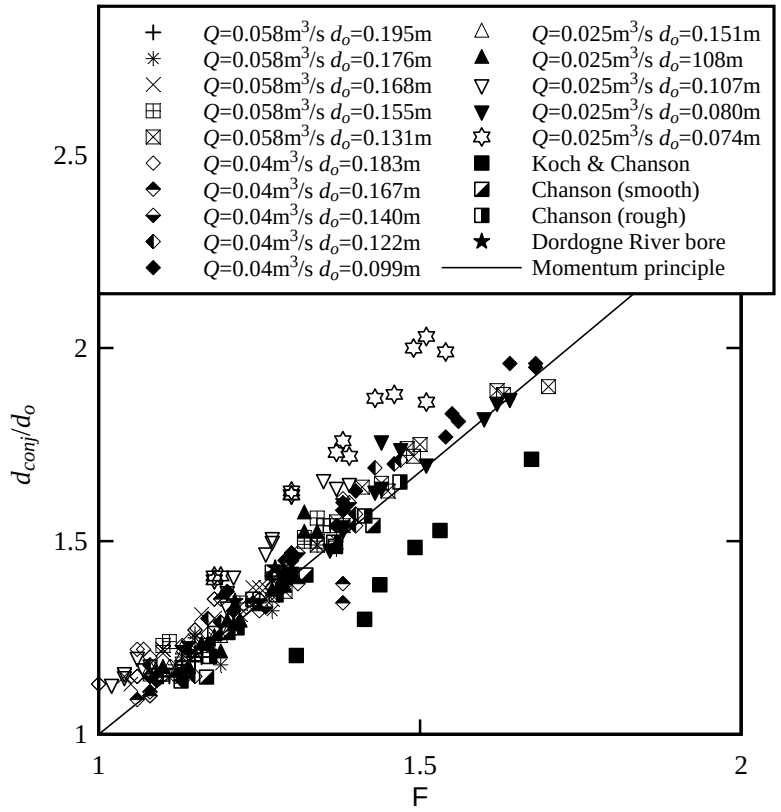


Fig.4 - Ratio of the conjugate depths in tidal bores - Comparison between the present data, the momentum equation (Eq. (1)), earlier laboratory studies (Koch and Chanson 2009, Chanson 2010) and a prototype study on the Dordogne River (Navarre 1995)

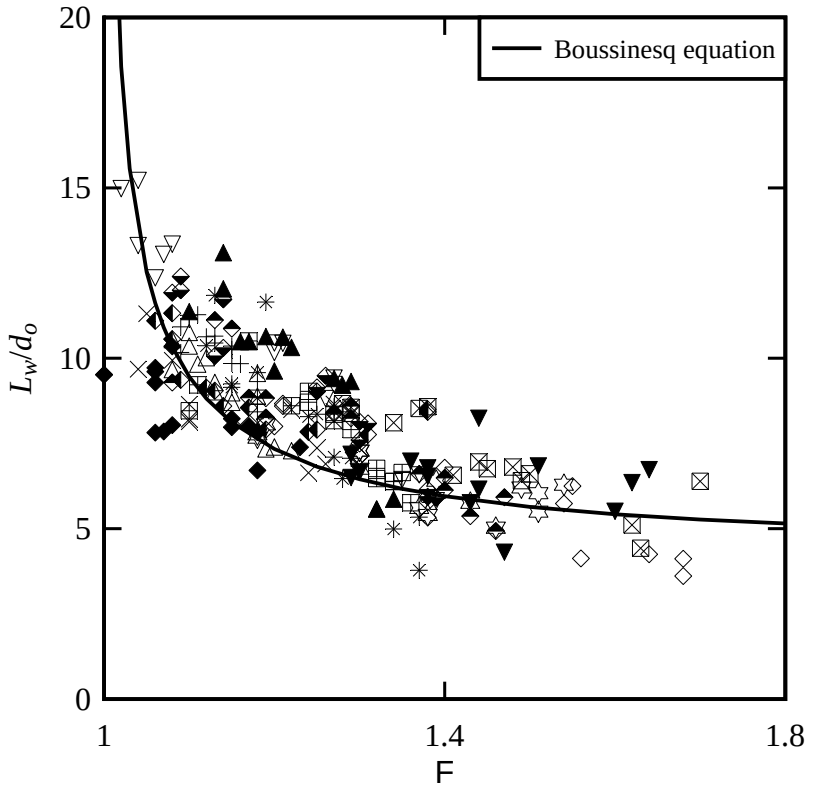


Fig.5 - Dimensionless wave length $L_w/d_o$ of the first wave length of undular tidal bores - Comparison between present data and the Boussinesq equation (Andersen 1978) - Same legend as Figure 4

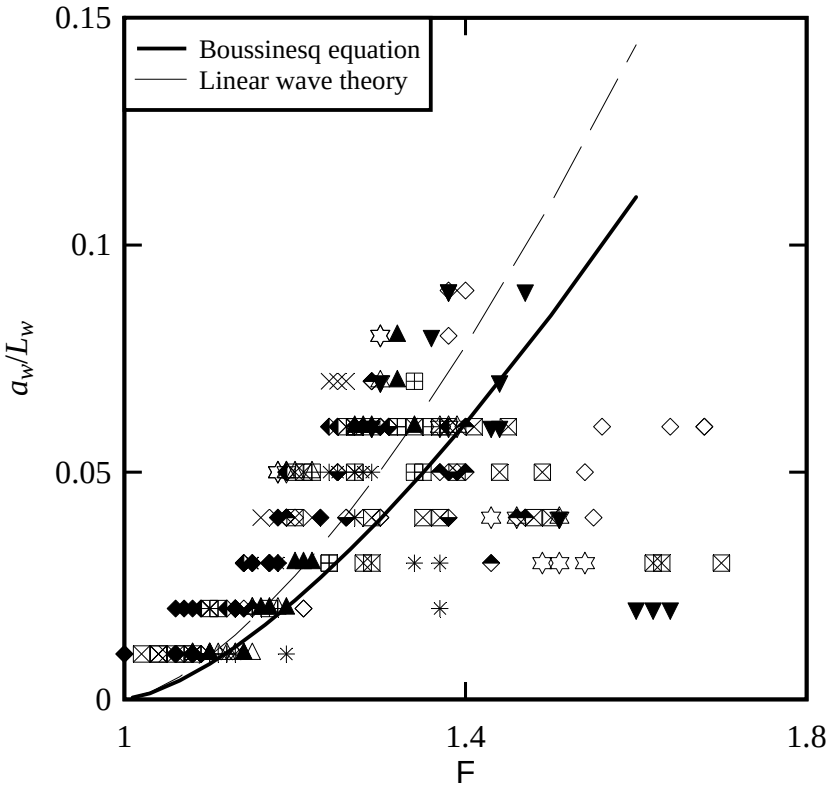


Fig. 6 - Dimensionless wave steepness $a_w/L_w$ of the first wave length of undular tidal bores - Comparison between present data, the Boussinesq equation (Andersen 1978) and the linear wave theory (Lemoine 1948) - Same legend as Figure 4

## 4. Particle trajectories

For one flow rate, the dispersion of light-weight particles was investigated in both undular and breaking tidal bores (Table 1). The particle trajectories were observed about $x$ = 5 m. Some typical particle trajectories are presented in Figures 7 and 8 for the undular and breaking tidal bores respectively. The particle trajectories are shown in a dimensionless form: for each trajectory, the horizontal axis is the longitudinal distance $x'$ positive downstream with $x' = 0$ when the particle passed underneath the leading edge of the bore front and the vertical axis is the particle vertical elevation $z$. The time interval between each data point is 1/30 s, and the tidal bore propagated from right to left on each graph.

In the undular bore, the particle trajectories highlighted two distinct trends. For the particles flowing initially in the upper flow region ($z_o/d_o > 0.5$), a relatively significant proportion followed a helicoidal pattern illustrated in Figure 7 (Particles 6a, 6c, 6d, 8b). These particles followed an orbital path beneath the wave crest, reaching their maximum vertical elevation just below the wave crests. Between wave crests, these particles were advected in the downstream direction as they passed underneath each wave trough. The particle orbital trajectories were comparable to the particle trajectories observed below regular waves (Sawaragi 1995), although the entire particle motion appeared to be a combination of orbital paths and downstream advection. Further regular waves cause only mild mixing which is very different from the intense mixing induced by the tidal bore. When the particles flowed initially close to the bed ($z_o/d_o < 0.5$), they were subjected to some recirculation motion consisting of an initially rapid deceleration followed by an upstream advection close to the bed behind the bore front. For example in Figure 7, the particles 2, 4c and 5b were recirculated upstream with an advective velocity $V_x/V_o$ = -0.5 in average. The two distinctive patterns are seen in Figure 7.

In the breaking bore, the particle trajectory motion was more complex. Most particles travelling initially next to the channel bed ($z_o/d_o < 0.2$) were subjected to a sudden deceleration followed by an upstream motion: e.g., the particle trajectory b8 with white circular symbols in Figure 8. The other particle trajectories exhibited a pseudo-chaotic motion induced by the large scale turbulent eddies generated in the mixing layer of the bore roller. Some examples of such particle trajectories are presented in Figure 8 (e.g. particles b2a, b6a, b9b, b10c). Note that the experiments were conducted for a relatively small Froude number for which the air entrainment in the breaking bore roller was negligible to small and did not affect adversely the particle tracking accuracy.

### 4.1 Particle mixing

The observations showed qualitatively a rapid mixing of the particles during the tidal bore passage. Assuming a homogenous, stationary turbulence behind the bore front, the turbulent diffusion coefficient of the particles may be estimated from their mean square displacement:

$$D_x = \frac{\sigma_x^2}{2\,t'} \quad (3)$$

$$D_z = \frac{\sigma_z^2}{2\,t'} \quad (4)$$

where $D_x$ and $D_z$ are the turbulent mixing coefficients of the particles in the $x$- and $z$-directions respectively, $\sigma_x$ and $\sigma_z$ are respectively the mean square displacement of the particles in the $x$- and $z$-directions, and $t'$ is the time scale with $t' = 0$ when the particle passed beneath the leading edge of the bore front. Equations (3) and (4) may be derived using Langevin's model of turbulent dispersion or the random walk model assuming that $t'$ is much larger than the Lagrangian time scale (Pope 2000, Chanson 2004). Simply $D_x$ and $D_z$ characterised the turbulent diffusion of the light-weight particles immediately behind the tidal bore front within the simplistic approximations of homogeneous turbulence and vertically-mixed water column.

CHANSON, H., and TAN, K.K. (2010). "Turbulent Mixing of Particles under Tidal Bores: an Experimental Analysis." *Journal of Hydraulic Research*, IAHR, Vol. 48, No. 5, pp. 641-649 (DOI: 10.1080/00221686.2010.512779 (ISSN 0022-1686).

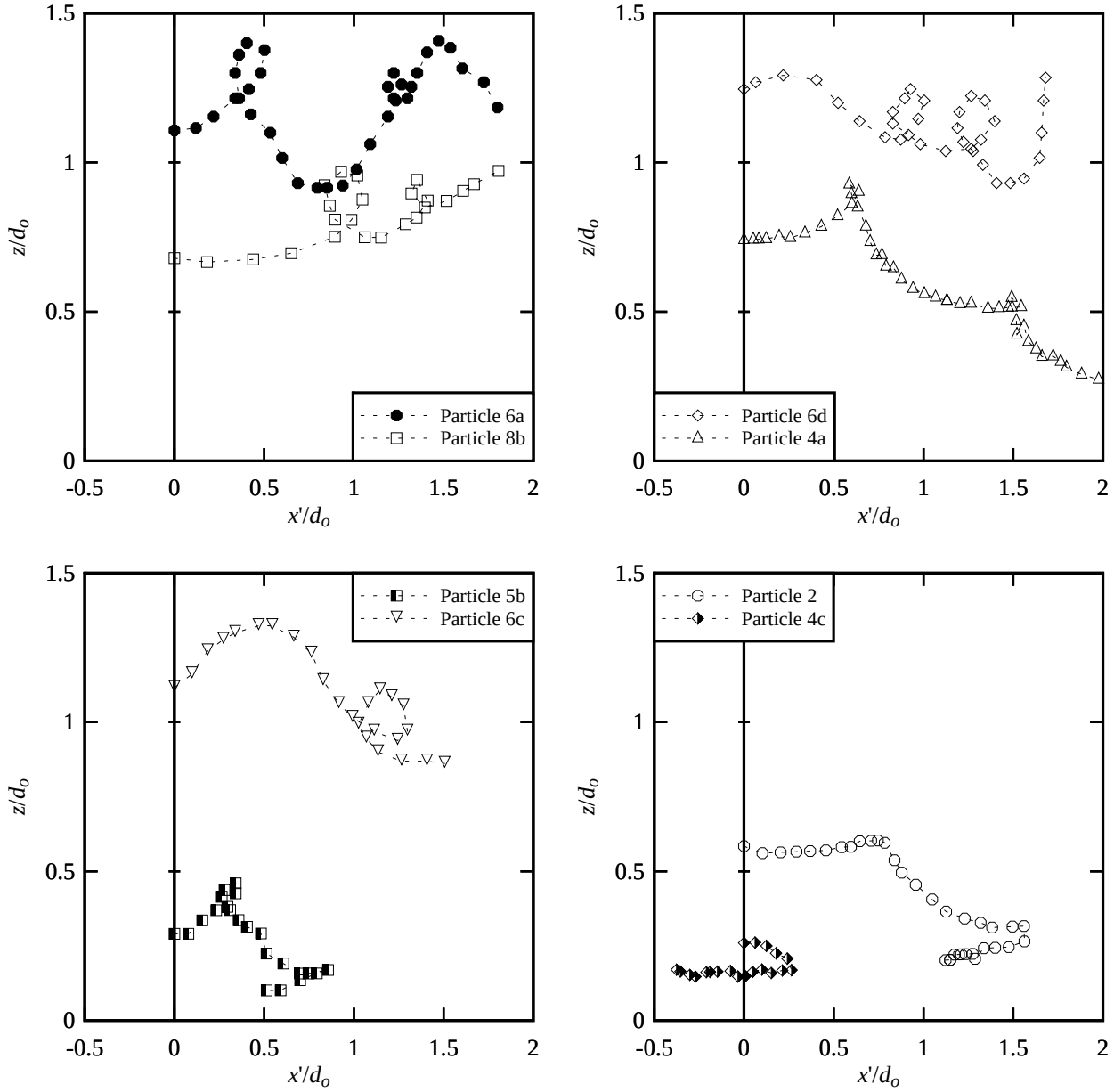


Fig. 7 - Dimensionless particle trajectories in an undular tidal bore: F = 1.15, $Q$ = 0.013 m$^3$/s, $d_o$ = 0.0775 m - Bore propagation from right to left

The dimensionless results are summarised in Table 2. Despite the simplistic assumptions underlying Equations (3) and (4), the data suggested that the longitudinal mixing coefficient was nearly one order of magnitude greater than the vertical mixing coefficient (Table 2). Further the undular bore induced a greater vertical mixing than the breaking bore, and it is believed to be linked with the streamline pattern induced by the free-surface undulations.

For comparison, the average vertical mixing coefficient in a fully-developed open channel is:

$$\frac{\varepsilon_z}{V_o d_o} = 0.067\sqrt{\frac{f}{8}} \quad (5)$$

where $f$ is the Darcy-Weisbach friction factor (Rutherford 1994, Chanson 2004); for a smooth flume, it yields $\varepsilon_z/(V_o d_o) \approx 0.003$ to 0.004. The present data implied that the vertical diffusion coefficients behind tidal bores were one order of magnitude larger than the vertical diffusion coefficient in a fully-developed, steady open channel flow. Overall the experimental data showed the strong longitudinal and vertical mixing during the tidal bore passage with moderate differences between undular and breaking tidal bores (Table 2).

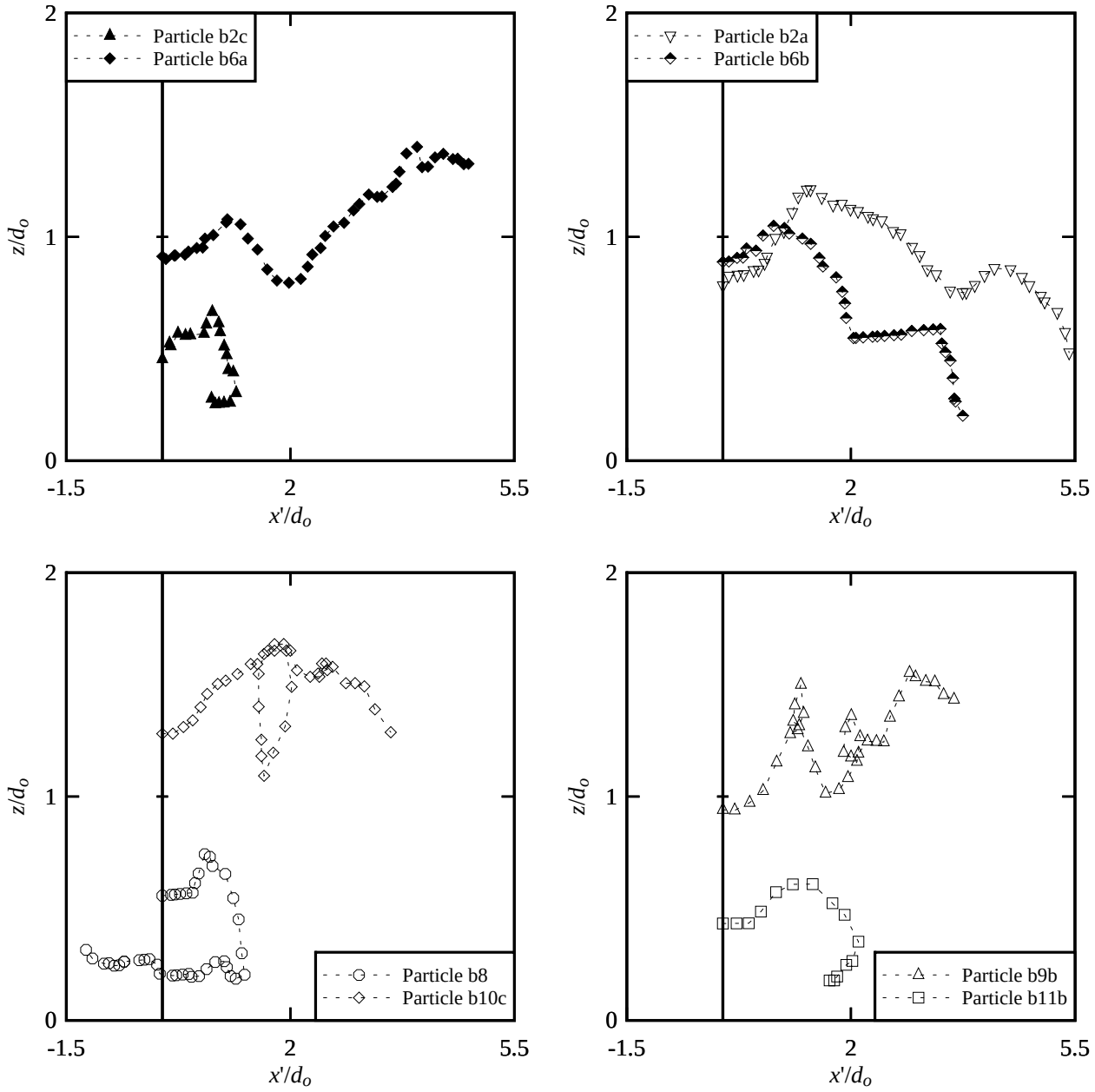


Fig. 8 - Dimensionless particle trajectories in a breaking tidal bore: F = 1.51, $Q$ = 0.013 m$^3$/s, $d_o$ = 0.0505 m - Bore propagation from right to left

Table 2 - Turbulent mixing coefficients of light-weight particles immediately behind tidal bores

| Tidal bore (1) | $V_o$ (m/s) (2) | $d_o$ (m) (3) | $D_x/(V_o d_o)$ (4) | $D_z/(V_o d_o)$ (5) | Remark (6) |
|---|---|---|---|---|---|
| Undular | 0.335 | 0.0775 | 0.10 | 0.018 | For $t\sqrt{g/d_o}$ <14 |
| Breaking | 0.515 | 0.0505 | 0.12 | 0.011 | |

## 5. Discussion

The present findings demonstrated a broad spectrum of particle trajectories and patterns during the passage of a tidal bore (Fig. 7 & 8). Both qualitative and quantitative observations implied the existence of large

scale vortices in which the particles were trapped and advected within. Earlier physical and numerical studies documented the production of large coherent structures in tidal bores (Koch and Chanson 2009, Lubin et al. 2010). The existence of energetic turbulent events beneath and shortly after the tidal bore front implied the generation of vorticity during the bore propagation. The presence of these persisting coherent structures indicated that a great amount of sediment materials could be placed into suspension and transported by the main flow in a natural system. The present observations with light-weight particles suggested that the tidal bore process contributes efficiently to the longitudinal dispersion of the eggs, reducing the efficiency of the predators in tidal-bore affected estuaries as proposed by Morris et al. (2003).

Beneath the undular tidal bore, the particle motion data yielded relatively large fluctuations of horizontal and vertical particle velocity components beneath the undulations. The long-lasting impact of the free-surface undulations is a key feature of undular tidal bores in natural systems (Koch and Chanson 2008). The comparative observations with a same initial flow rate suggested that the undular bore induced a greater particle mixing compared to the breaking bore especially in the upper flow region ($z_o/d_o$ > 0.5) (Table 2, column 5).

The present results may provide a better understanding of the impact of tidal bore on fish eggs in a tidal bore affected estuary. In the natural system, the fish eggs are typically advected downstream by the ebb tide. The arrival of the tidal bore does induce a marked longitudinal spread of the eggs. Those located in the upper flow region continue to flow downstream, while the others reverse their course being re-directed upstream behind the bore. The tidal bore induces a very rapid longitudinal spread of the eggs with some form of preferential motion depending upon their vertical position in the water column. The lowest, typically heaviest fish eggs are advected upstream immediately after the tidal bore passage. The higher, typically neutrally buoyant eggs located next to the surface continue their journey downstream for sometimes, although the strong flood flow may bring them back into the upper estuary at a later stage of the tide.

## 7. Conclusion

The present study investigated the turbulent mixing of light-weight particles in a tidal bore. Herein the small particles had some physical properties close to striped bass fish eggs, and their turbulent dispersion associated with the passage of undular and breaking bores was documented experimentally.

The free-surface properties were investigated for a range of initial flow conditions (Table 1). The findings suggested that the initial flow properties had little effect on the tidal bore characteristics. The undular wave steepness data highlighted a local maximum for $F$ = 1.3 to 1.4 that was associated with the apparition of some breaking at the first wave crest, and the disappearance of the secondary waves for $F$ > 1.5 to 1.6. The results highlighted that the initial flow conditions had little effects on the dimensionless free-surface properties.

The particle trajectory data complemented some earlier experimental and numerical results: they showed in particular some rapid particle deceleration and reversal beneath the bore front. Some large fluctuations of horizontal and vertical particle velocities were observed during the undular bore passage and beneath the ensuing the undulations. Some seminal features were highlighted, including some large-scale motion highlighting the existence of large coherent vortical structures. These large turbulent eddies are responsible for some bed erosion and vertical mixing of the water column when a tidal bore propagates upstream in the estuarine zone of a natural system. The large-scale vortices are also responsible to the longitudinal dispersion of fish eggs reducing the impact of predators. The present results showed that the tidal bore induces a very rapid longitudinal spread of the eggs with some form of preferential motion depending upon their initial vertical elevation $z_o/d_o$.

Finally it must be noted that the present experiments were performed with an unique particle size and density. Future tests should encompass a range of particle sizes and density.

## 8. Acknowledgments

The authors acknowledge the technical assistance of Graham Illidge and Clive Booth (University of Queensland).

CHANSON, H., and TAN, K.K. (2010). "Turbulent Mixing of Particles under Tidal Bores: an Experimental Analysis." *Journal of Hydraulic Research*, IAHR, Vol. 48, No. 5, pp. 641-649 (DOI: 10.1080/00221686.2010.512779 (ISSN 0022-1686).

## 9. Notation

| | |
|---|---|
| $a_w$ | amplitude (m) of the first wave length; |
| $B$ | channel width (m); |
| $d$ | flow depth (m) measured normal to the invert; |
| $D_x$ | turbulent mixing coefficient ($m^2/s$) in the x-direction; |
| $D_z$ | turbulent mixing coefficient ($m^2/s$) in the z-direction; |
| $\mathsf{F}$ | tidal bore Froude number: $\mathsf{F} = (V_o + U)/\sqrt{g\ d_o}$ ; |
| $f$ | Darcy-Weisbach friction factor; |
| $g$ | gravity constant: $g = 9.80$ m/s$^2$ in Brisbane, Australia; |
| $L_w$ | wave length (m) of the first wave length; |
| $Q$ | volume flow rate ($m^3/s$); |
| $s$ | particle relative density |
| $t$ | time (s); |
| $t'$ | time (s) with $t' = 0$ when the particle passed beneath the bore front; |
| $U$ | bore front celerity (m/s); |
| $V$ | velocity (m/s); |
| $V_o$ | initial flow velocity (m/s); |
| $w_s$ | particle fall velocity (m/s); |
| $x$ | longitudinal distance (m) measured from the channel upstream end; |
| $x'$ | longitudinal distance (m) with $x' = 0$ when the particle passed beneath the bore front; |
| $z$ | particle elevation (m) above the invert; |
| $z_o$ | initial particle elevation (m) above the invert (at $t' = 0$); |
| $\varepsilon_z$ | vertical mixing coefficient ($m^2/s$) in fully-developed open channel flows; |
| $\sigma_x$ | mean square displacement (m) of particles in the x-direction; |
| $\sigma_z$ | mean square displacement (m) of particles in the z-direction; |

*Subscript*

| | |
|---|---|
| *conj* | conjugate flow conditions; |
| *o* | initial flow conditions prior to the bore passage; |
| *x* | longitudinal component |
| *z* | vertical component. |

## References

Andersen, V.M. (1978). Undular Hydraulic Jump. *Journal of Hydraulic Division*, ASCE, Vol. 104, No. HY8, pp. 1185-1188. Discussion : Vol. 105, No. HY9, pp. 1208-1211.

Barré de Saint-Venant, A.J.C. (1871). Théorie du Mouvement Non Permanent des Eaux, avec Application aux Crues des Rivières et à l'Introduction des Marées dans leur Lit. ('Theory of Unsteady Flow Motion, including Applications to Floods and Tidal Effect.') *Comptes Rendus des séances de l'Académie des Sciences*, Paris, France, Vol. 73, No. 4, pp. 147-154 (in French).

Bazin, H. (1865). Recherches Expérimentales sur la Propagation des Ondes. ('Experimental Research on Wave Propagation.') *Mémoires présentés par divers savants à l'Académie des Sciences*, Paris, France, Vol. 19, pp. 495-644 (in French).

Benet, F., and Cunge, J.A. (1971). Analysis of Experiments on Secondary Undulations caused by Surge Waves in Trapezoidal Channels. *Journal of Hydraulic Research*, IAHR, Vol. 9, No. 1, pp. 11-33.

Benjamin, T.B., and Lighthill, M.J. (1954). On Cnoidal Waves and Bores. *Proc. Royal Soc. of London, Series A, Math. & Phys. Sc.*, Vol. 224, No. 1159, pp. 448-460.

Boussinesq, J.V. (1877). Essai sur la Théorie des Eaux Courantes. ('Essay on the Theory of Water Flow.') *Mémoires présentés par divers savants à l'Académie des Sciences*, Paris, France, Vol. 23, Série 3, No. 1, supplément 24, pp. 1-680 (in French).

British Standard (1943). Flow Measurement. *British Standard Code BS 1042:1943*, British Standard Institution, London.

CHANSON, H., and TAN, K.K. (2010). "Turbulent Mixing of Particles under Tidal Bores: an Experimental Analysis." *Journal of Hydraulic Research*, IAHR, Vol. 48, No. 5, pp. 641-649 (DOI: 10.1080/00221686.2010.512779 (ISSN 0022-1686).

Chanson, H. (2004). Environmental Hydraulics of Open Channel Flows. *Elsevier-Butterworth-Heinemann*, Oxford, UK, 483 pages.

Chanson, H. (2010). Unsteady Turbulence in Tidal Bores: the Effects of Bed Roughness. *Journal of Waterway, Port, Coastal, and Ocean Engineering*, ASCE, Vol. 136 (In print).

Cunge, J.A. (2003). Undular Bores and Secondary Waves - Experiments and Hybrid Finite-Volume Modelling. *Journal of Hydraulic Research*, IAHR, Vol. 41, No. 5, pp. 557-558.

Favre, H. (1935). Etude Théorique et Expérimentale des Ondes de Translation dans les Canaux Découverts. ('Theoretical and Experimental Study of Travelling Surges in Open Channels.') *Dunod*, Paris, France (in French).

Henderson, F.M. (1966). Open Channel Flow. *MacMillan Company*, New York, USA.

Hornung, H.G., Willert, C., and Turner, S. (1995). The Flow Field downstream of a Hydraulic Jump. *Jl of Fluid Mech.*, Vol. 287, pp. 299-316.

Koch, C., and Chanson, H. (2008). Turbulent Mixing beneath an Undular Bore Front. *Journal of Coastal Research*, Vol. 24, No. 4, pp. 999-1007 (DOI: 10.2112/06-0688.1).

Koch, C., and Chanson, H. (2009). Turbulence Measurements in Positive Surges and Bores. *Journal of Hydraulic Research*, IAHR, Vol. 47, No. 1, pp. 29-40 (DOI: 10.3826/jhr.2009.2954).

Lemoine, R. (1948). Sur les Ondes Positives de Translation dans les Canaux et sur le Ressaut Ondulé de Faible Amplitude. ('On the Positive Surges in Channels and on the Undular Jumps of Low Wave Height.') *Jl La Houille Blanche*, Mar-Apr., pp. 183-185 (in French).

Liggett, J.A. (1994). Fluid Mechanics. *McGraw-Hill*, New York, USA.

Lubin, P., Glockner, S., and Chanson, H. (2010). Numerical Simulation of a Weak Breaking Tidal Bore. *Mechanics Research Communications*, Vol. 37, No. 1, pp. 119-121 (DOI: 10.1016/j.mechrescom.2009.09.008).

Montes, J.S., and Chanson, H. (1998). Characteristics of Undular Hydraulic Jumps. Results and Calculations. *Journal of Hydraulic Engineering*, ASCE, Vol. 124, No. 2, pp. 192-205.

Morris, J.A., Rulifson, R.A., and Toburen, L.H. (2003). Life History Strategies of Striped Bass, *Morone Saxatilis*, Populations inferred from Otolith Microchemistry. *Fisheries Research*, Vol. 62, pp. 53-63.

Navarre, P. (1995). Aspects Physiques du Caractère Ondulatoire du Macaret en Dordogne. ('Physical Features of the Undulations of the Dordogne River Tidal Bore.') *D.E.A. thesis*, Univ. of Bordeaux, France, 72 pages (in French).

Peregrine, D.H. (1966). Calculations of the Development of an Undular Bore. *Jl. Fluid Mech.*, Vol 25, pp.321-330.

Pope, S.B. (2000). Turbulent Flows. *Cambridge University Press*, UK, 771 pages.

Rayleigh, Lord (1908). Note on Tidal Bores. *Proc. Royal Soc. of London, Series A containing Papers of a Mathematical and Physical Character*, Vol. 81, No. 541, pp. 448-449.

Rouse, H. (1946). Elementary Mechanics of Fluids. *John Wiley & Sons*, New York, USA, 376 pages.

Rulifson, R.A., and Tull, K.A. (1999). Striped Bass Spawning in a Tidal Bore River: the Shubenacadie Estuary, Atlantic Canada. *Trans. American Fisheries Soc.*, Vol. 128, pp. 613-624.

Rutherford, J.C. (1994). River Mixing. *John Wiley*, Chichester, USA, 347 pages.

Sawaragi, T. (1995). Coastal Engineering - Waves, Beaches, Wave-Structure Interactions. *Elsevier*, Developments in Geotechnical Engineering Series, No. 78, Amsterdam, The Netherlands, 479 pages.

Treske, A. (1994). Undular Bores (Favre-Waves) in Open Channels - Experimental Studies. *Journal of Hydraulic Research*, IAHR, Vol. 32, No. 3, pp. 355-370. Discussion: Vol. 33, No. 3, pp. 274-278.